Static Recrystallization Phase-Field Simulation Based on The Predicted Subgrain Structures

T. Takaki[1]*, A. Yamanaka[2], Y. Tomita[3]

[1] *Graduate School of Science and Technology, Kyoto Institute of Technology, Matsugasaki, Sakyo, Kyoto, 606-8585, Japan*
[2] *Graduate School of Science and Technology, Kobe University, 1-1, Rokkodai, Nada, Kobe, 657-8501, Japan*
[3] *Graduate School of Engineering, Kobe University, 1-1, Rokkodai, Nada, Kobe, 657-8501, Japan*
e-mail: takaki@mech.kit.ac.jp, yamanaka@solid.mech.kobe-u.ac.jp, tomita@mech.kobe-u.ac.jp

Abstract In this study, a coupled model that estimates recrystallization kinetics and structure is developed by employing a phase-field method and crystal plasticity theory. In this model, the deformation subgrain structure which is the initial structure of recrystallization simulation is predicted from the stored energy and crystal orientation calculated from crystal plasticity finite element simulation. Then, based on the predicted subgrain structures, static recrystallization are simulated by multi-phase-field method taking account of the orientation dependence of boundary energy and mobility. The model developed in this study enable to consider the deformation structures and the spontaneous nucleation through the abnormal subgrain growth, unlike the conventional model driven by the stored energy and using the nucleation criteria.

Key words: Static Recrystallization, Multi-Phase-Field Method, Subgrain Structure, Abnormal Subgrain Growth, Crystal Plasticity, Coupled Simulation

INTRODUCTION

The development of recrystallization model is essential to predict the recrystallization texture, microstructure and kinetics during annealing. There are some computational models for recrystallization [1], such as vertex or network model, Monte Carlo Potts model [2], cellular automata model [3] and phase-field model [4, 5]. In all these models, the introduction of the realistic deformation microstructure which is the initial structure of recrystallization simulation is indispensable for the accurate estimations of recrystallization process. Therefore, the deformation microstructures are obtained experimentally [6] or numerically [7].

There are two types of recrystallization model: One is the grain growth model driven by the stored energy [4, 6, 7], in which the deformation microstructure is characterized by the crystal orientation and stored energy. Since this model needs nucleation criteria, the calculated recrytallization kinetics and structure change depending on the predefined nucleation conditions. The other model describes grain growth by the balance of grain boundary energies, and considers the subgrain structure in which there are no dislocations inside individual subgrain [5]. Although this model requires smaller computational grids and much computational cost comparing to the first model in order to express subgrain microstructures, by introducing the misorientation dependence of boundary energies and mobility to the model, the natural nucleation of recrystallized grains is enabled through the abnormal grain growth [8].

In this study, we develop a coupled model for static recrystallization of a phase-field method that describes second model mentioned above and crystal plasticity finite element method. Since the normal crystal plasticity finite element simulation never give subgrain microstructures, the subgrain structures are predicted from crystal orientation and stored energy calculated by the deformation simulation. The multi-phase-field model of Steinbach et al. [9] is employed as a grain growth model and the misorientation dependency of grain boundary energies and mobility are introduced into the phase-field model.

This paper consists of five chapters: Following this introduction, a multi-phase-field model for grain growth and algorithm for the efficient computation are described. Next, we explain the procedure of recrystallization model developed in this study. In chapter of numerical results, first, the effects of misorientation and inhomogeneous deformation on subgrain growth are confirmed by using simple polycrystalline model, and then the results for every step following the developed recrystallization model are shown in detail. And, we discuss the capability of the developed model against the predictability of real processes. Finally we conclude this study.

PHASE-FIELD MODEL

In grain growth simulation during recrystallization, the multi-phase-field model of Steinbach et al. [9] is employed. This model has an advantage that the phase field parameters, such as gradient coefficient and phase field mobility, can be perfectly related to the grain boundary energy and mobility with misorientation dependency. Furthermore, this model removes some difficulties in the treatment of triple points or higher order interactions. The computational difficulties caused by using many phase field variables are overcome by employing an efficient algorism of Kim et al. [10].

1. Multi-phase-field model Considering a system containing N different grains ϕ_1, ϕ_2,.... ϕ_N, the free energy functional can be taken as

$$F = \int_V \left[\sum_{\alpha=1}^{N} \sum_{\beta=\alpha+1}^{N} \left(-\frac{a_{\alpha\beta}^2}{2} \nabla\phi_\alpha \cdot \nabla\phi_\beta + W_{\alpha\beta}\phi_\alpha\phi_\beta \right) \right] dV , \tag{1}$$

where, $a_{\alpha\beta}$ and $W_{\alpha\beta}$ are the gradient coefficient and the height of double well potential between α-th and β-th grains. The phase field ϕ_α takes a value of 1 inside the α-th grain, 0 inside other grains, and $0 < \phi_\alpha < 1$ at grain boundary. ϕ_α is not an independent variable and must satisfy the following condition:

$$\sum_{\alpha=1}^{N} \phi_\alpha = 1 . \tag{2}$$

Here, we define a step function σ_α with $\sigma_\alpha = 1$ if $0 < \phi_\alpha < 1$ and $\sigma_\alpha = 0$ elsewhere. Using this step function, the number of locally present phases n is expressed as

$$n = \sum_{\alpha=1}^{N} \sigma_\alpha(x,t) . \tag{3}$$

Using Eq. 3, N in Eqs. 1 and 2 can be replaced by n.

Following Ref. 9, the time evolution equation of phase field is obtained as

$$\dot{\phi}_i = -\sum_{j=1}^{n} \frac{M_{ij}^{\phi}}{n} \left(\frac{\delta F}{\delta \phi_i} - \frac{\delta F}{\delta \phi_j} \right) = -\sum_{j=1}^{n} \frac{M_{ij}^{\phi}}{n} \left[\sum_{k=1}^{n} \left\{ \left(W_{ik} - W_{jk} \right) \phi_k + \frac{1}{2} \left(a_{ik}^2 - a_{jk}^2 \right) \nabla^2 \phi_k \right\} \right] , \tag{4}$$

where i, j and k are the local grain number from 1 to n at a numerical grid point.

2. Phase field parameters The phase-field parameters are related to the material parameters as follows [11]:

$$W_{ij} = \frac{4\gamma_{ij}}{\delta} , \; a_{ij} = \frac{2}{\pi}\sqrt{2\delta\gamma_{ij}} \;\text{ and }\; M_{ij}^{\phi} = \frac{\pi^2}{4\delta} M_{ij} , \tag{5}$$

where δ is the grain boundary thickness and γ_{ij} and M_{ij} are the grain boundary energy and mobility between i-th and j-th grains. To introduce the misorientation dependency of grain boundary energy and mobility, the following equations are used [8].

$$\gamma_{ij}\left(\Delta\theta_{ij}\right) = \gamma_m \frac{\Delta\theta_{ij}}{\Delta\theta_m} \left(1 - \ln \frac{\Delta\theta_{ij}}{\Delta\theta_m} \right) . \tag{6}$$

$$M_{ij}\left(\Delta\theta_{ij}\right)=M_m\left[1-\exp\left\{-5\left(\frac{\Delta\theta_{ij}}{\Delta\theta_m}\right)^4\right\}\right]. \tag{7}$$

Here, $\Delta\theta_{ij}$ is the misorientation between i-th and j-th grains, γ_m and M_m are respectively the boundary energy and mobility at $\Delta\theta_{ij} = \Delta\theta_m$ which is the misorientation when the boundary becomes a high angle boundary. The variations in grain boundary energy and mobility with misorientation expressed by Eqs. 6 and 7 are illustrated in Fig. 1.

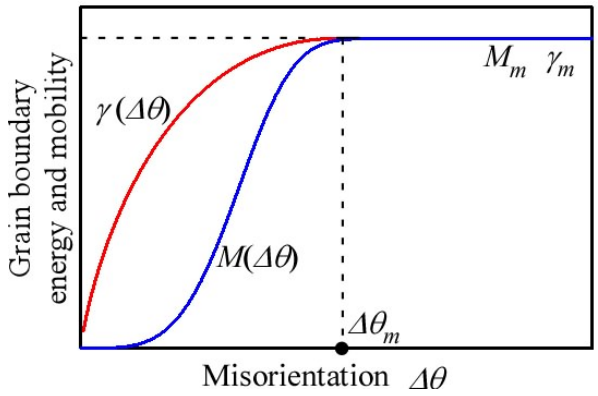

Fig. 1 Misorientation dependency of grain boundary energy and mobility expressed by Eqs. 6 and 7

3. Algorithm for efficient computation As we can see from Eq. 4, we do not have to solve Eq. 4 on the grid points with $n = 1$ and it is sufficient to save the values of not N but n phase fields. Furtheremore, by introducing the following algorithm [10], we can solve Eq. 4 very efficiently.

(1) Solve Eq. 4 for n phase fields.

(2) During (1), if ϕ_i at previous time step is zero and the calculated increment $\Delta\phi_i$ has a minus value, i-th phase field is put away from the phase field group on the grid point. And, steps (1) and (2) are repeated until all phase fields satisfied above condition are removed.

(3) The phase fields are rearranged in the order of largest to smallest. Phase fields from the largest until n_ϕ-th are recorded. Here, n_ϕ is a predefined maximum number of the recorded phase field.

(4) The phase fields are replaced by following $\phi_i^* = \phi_i \Big/ \sum_{j=1}^{n_\phi} \phi_j$ so as to satisfy $\sum_{i=1}^{n_\phi} \phi_i^* = 1$.

(5) If a phase field is not saved at a grid point of (l, m) and its value at grid points of $(l\pm1, m\pm1)$, or the nearest four neighbors, is not zero, the phase field is added to the phase field group on the grid (l, m). Therefore, the number of phase fields solved in the step (1) sometime becomes more than n_ϕ.

Although this algorithm basically follows Ref. [10], the iteration in steps (1) and (2) is added to achieve higher accuracy.

RECRYSTALLIZATION COUPLED MODEL

When we obtain the stored energy E_{store} from subgrain structures measured experimentally, such as EBSD method, we often use the equation

$$E_{store}=\frac{K\gamma_s}{D_s}, \tag{8}$$

where γ_s is the grain boundary energy, D_s is the subgrain diameter and K is a constant depending on the space dimension [12]. Since, in crystal plasticity finite element simulation, the stored energy can be calculated by

$$E_{store}=\frac{1}{2}\rho\mu b^2, \tag{9}$$

where ρ is the dislocation density, μ is the shear modulus and b is the magnitude of Burgers vector, the subgrain diameter can be calculated as

$$D_s = \frac{K}{E_{store}}\gamma_s = \frac{K}{E_{store}}\gamma_m \frac{\Delta\theta}{\Delta\theta_m}\left(1 - \ln\frac{\Delta\theta}{\Delta\theta_m}\right), \tag{10}$$

where Eq. 6 is substituted. However, usually it is impossible to obtain the misorientation $\Delta\theta$ directly from crystal plasticity finite element simulation. Furthermore, in the case using triangular element in finite element simulation, the stored energy and crystal orientation are constant inside individual element and abruptly change between neighboring two triangular elements as a step function. Therefore, the smoothing operation is carried out using the equation

$$\theta^{(l,m)} = \sum_{p=1}^{q}\theta_p w_p \Big/ \sum_{p=1}^{q} w_p , \tag{11}$$

where $\theta^{(l,m)}$ is the smoothed orientation at a grid point (l, m) shown in Fig. 2, q is the number of grid points used in the smoothing operation (or the number of grid points located inside dashed circle with radius R_s in Fig. 2), θ_p is the crystal orientation at local point p, and w_p is a weight function expressed by $1/r_p$, where r_p is the distance between points (l, m) and p. The same operation is performed for stored energy. From the smoothed orientation, the amount of local orientation gradients $|\nabla\theta|$ are calculated at all grid points. Assuming $\Delta\theta = |\nabla\theta| D_s$ as shown in Fig. 3, from Eq. 10, the misorientation $\Delta\theta$ can be calculated using the local orientation gradient $|\nabla\theta|$ and smoothed stored energy E_{store} as

$$\Delta\theta = \Delta\theta_m \exp\left[1 - 1\Big/\left\{|\nabla\theta|\frac{K}{E_{stoer}}\frac{\gamma_m}{\Delta\theta_m}\right\}\right]. \tag{12}$$

Here, we summarize the recrystallization model developed in this study:

(1) Crystal orientation and stored energy of deformed polycrystalline material are calculated through crystal plasticity finite element simulation.

(2) The crystal orientation and stored energy are smoothed on the regular grids for phase-field simulation following Eq. 11.

(3) The amount of local orientation gradient $|\nabla\theta| = \sqrt{(\partial\theta/\partial x)^2 + (\partial\theta/\partial y)^2}$ is calculated on all grid points.

(4) The misorientation $\Delta\theta$ is calculated by Eq. 12 using the smoothed stored energy and local orientation gradient.

(5) Subgrain size at all grid points is determined using Eq. 10.

(6) Nuclei to generate the subgrain structure are seeded on the regular grids for phase-field simulation taking into account the calculated subgrain size.

(7) Subgrain structures are prepared by performing a normal grain growth simulation from the nuclei.

(8) Recrystallization phase-field simulation is carried out from the initial subgrain structure.

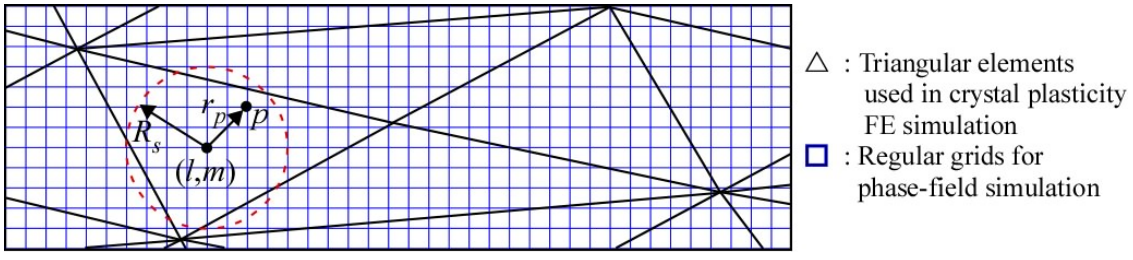

Fig. 2 Schematical illustration of relationship between triangle finite element and regular grids

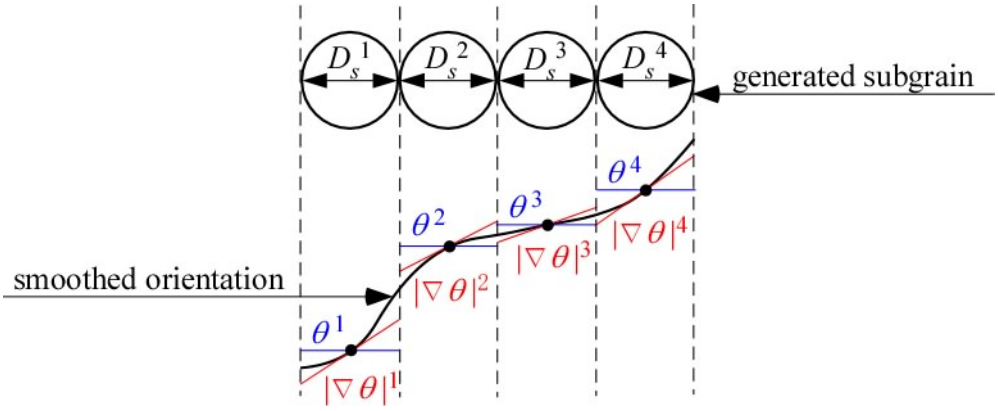

Fig. 3 Schematical illustration of relationship between smoothed orientation and predicted subgrain

NUMERICAL RESULTS

1. Abnormal subgrain growth The effects of misorientation and inhomogeneous deformation on the subgrain growth are investigated using simple polycrystalline model. Figure 4 show the initial subgrain structures used here. There are four hexagonal grains that are classified by coloring and of which boundaries are high-angle boundaries. Here, periodic boundary conditions are applied to the all sides of computational domain. Model A has 718 subgrains with almost same diameter of D_{ave} = 0.94 μm. Models B and C have two kinds of subgrain size. In model B with 657 subgrains, only central red grain has small subgrains of D_{ave} = 0.80 μm and the other three grains have large subgrains D_{ave} = 1.07 μm. On the other hand, in model C with 846 subgrains, central red grain has large subgrains of D_{ave} = 1.07 μm and the other grains have small subgrains of D_{ave} = 0.80 μm. The computational domain size is $500\Delta x \times 394\Delta x$ where grid size is Δx = 0.05 μm. The other conditions are as follows: the interface thickness $\delta = 7\Delta x$, interface energy γ = 1 J/m^2, time increment Δt = 0.0075 s and grain boundary mobility $M = M_0\exp(-Q/kT)$ where pre-exponential factor M_0 = 6.2x10^{-6} m^2/Ns, activation energy Q = 2.08x10^{-19} J, Boltzmann constant k = 1.38x10^{-23} J/K and temperature T = 800 K [13].

Figures 5 (a), (b) and (c) show the time slices of subgrain microstructual evolution for Model A with different misorientations $\Delta\theta$. In Fig. 5 (c), normal grain growth is observed, because all boundaries are high-angle boundary. On the other hand, in Fig. 5 (a), only grain boundaries with high-angle misorientation migrate, or the abnormal grain growth is observed. In Fig. 5 (b), intermediate behaviors of (a) and (c) can be observed: although the migrations of initial high-angle grain boundaries are prominent, the coarsening of subgrains inside initial grain is also occurred.

Figures 6 (a) and (b) demonstrate the time evolution of subgrain structures for Model B and C, respectively. In Models B and C, the deformation inhomogeneity is simply modeled by changing the subgrain size. Although , in Fig. 5 (a), the high-angle grain boundaries migrate into both grains with same subgrain structures, in Figs. 6 (a) and (b), those migrate only into the grain with smaller subgrains or larger deformation. Therefore, we can confirm that the present model can reproduce the experimental fact that recrystallization occurs much faster in highly deformed grain than lower one.

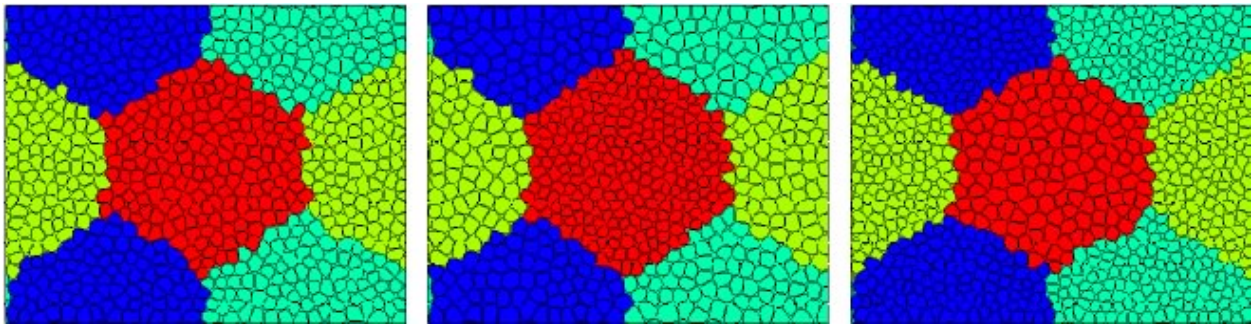

(a) Model A *(b) Model B* *(c) Model C*

Fig. 4 Initial subgrain structures with four hexagonal grains

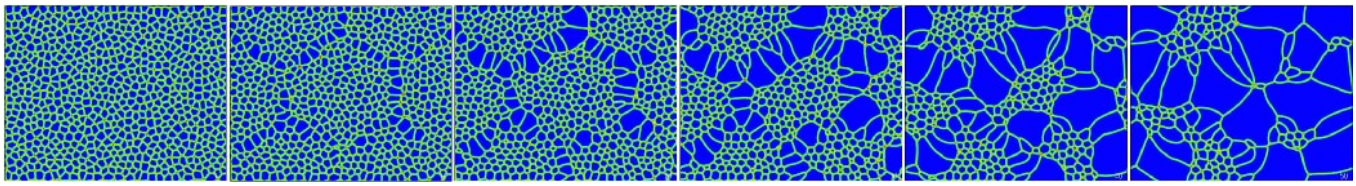

(a) $\Delta\theta$ = 4 degree

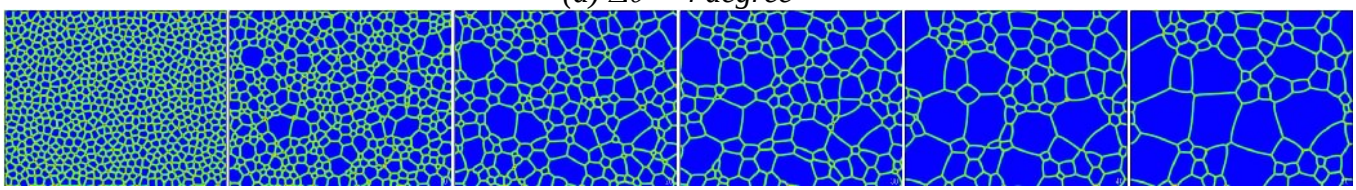

(b) $\Delta\theta$ = 7 degree

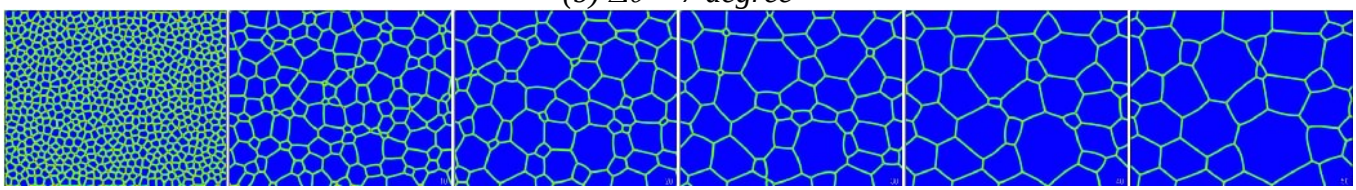

(c) $\Delta\theta$ > 15 degree

Fig. 5 Time evolution of subgrain structures for Model A. t = 7.5, 75, 150, 225, 300 and 375 s from left.

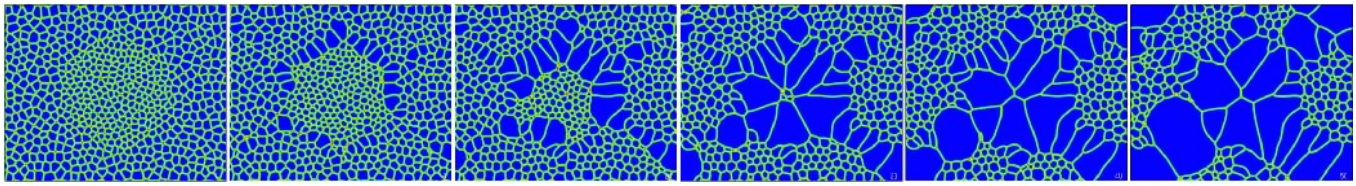

(a) Model B

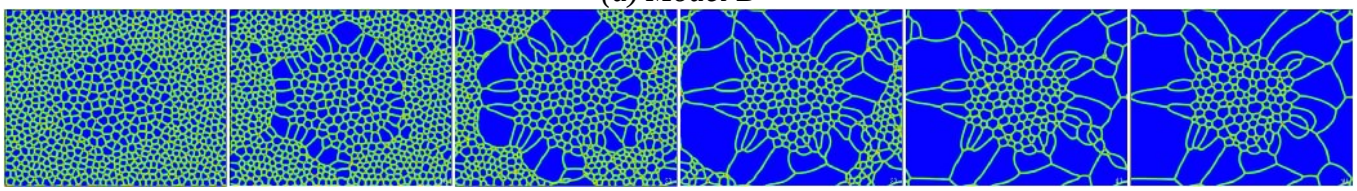

(b) Model C

Fig. 6 Time evolution of subgrain structures for models B and C in the case of $\Delta\theta$ = 4 degree. *t = 7.5, 75, 150, 225, 300 and 375 s from left.*

2. Recrystallization simulation Following the procedure of recrystallization model described in previous chapter, recrystallization simulation taking into account deformation microstructures is performed and the results in each computational step are shown in detail.

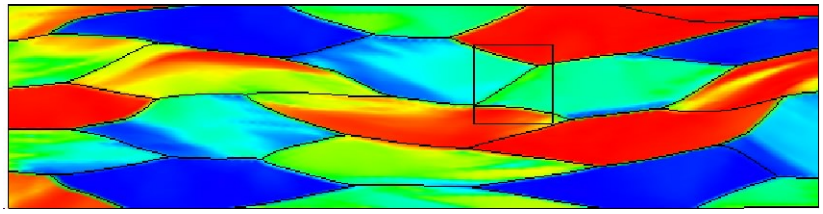

Fig. 7 Crystal orientation distributions at 50% compression by crystal plasticity finite element simulation [14]

Figure 7 shows the crystal orientation distributions at 50% compression calculated by crystal plasticity finite element simulation. The used crystal plasticity theory and numerical conditions are shown in Ref. [14]. In Fig. 7, the solid lines indicate the grain boundaries before deformation. Here, we use the square region of 80 μm x 80 μm in Fig. 7 as a computational domain for recrystallization simulation. This region has 626 triangle elements and is divided into 800 x 800 finite difference grids. The close-up views of square region in Fig. 7 are illustrated in Fig. 8. Since, in crystal plasticity finite element simulation, crossed triangle elements are employed, (a) crystal orientation and (b) stored energy are colored element by

element. The misorientation shown in Fig. 8 (c) indicates the orientation difference of neighboring two triangle elements.

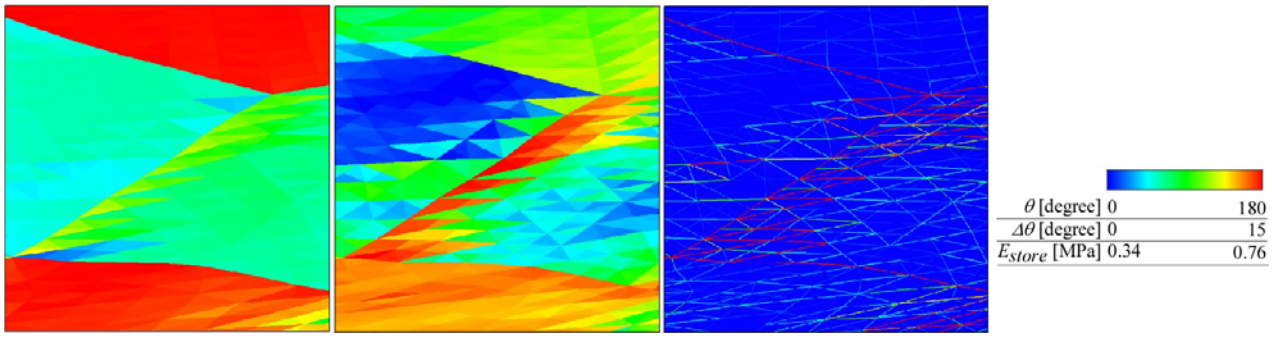

(a) *(b)* *(c)*

Fig. 8 Close-up views of square region in Fig. 7: (a) crystal orientation θ, (b) stored energy E_{store} and (c) misorientation $\Delta\theta$

Figures 9 (a) and (b) are the smoothed orientation and stored energy, respectively. The smoothing is carried out using Eq. 11 with $R_s = 3\Delta x$. In this case, since the R_s is relatively small, the smoothed regions are limited around sides of triangular elements. Next, the magnitude of orientation gradient at grid point (l,m) is calculated by $|\nabla\theta|_{(l,m)} = \frac{1}{2\Delta x}\sqrt{\left(\theta_{(l+1,m)} - \theta_{(l-1,m)}\right)^2 + \left(\theta_{(l,m+1)} - \theta_{(l,m-1)}\right)^2}$ using smoothed orientation. Then, using smoothed stored energy shown in Fig. 9 (b) and calculated gradient $|\nabla\theta|$, the misorientations on all grid points can be obtained from Eq. 12. The calculated misorientation distributions are shown in Fig. 9 (c). Here, the minimum misorientation is set to be 4 degrees, because we need very small numerical grid in order to reproduce small subgrain structures caused by small misorientation angle, as can be seen from Eq. 10. Comparing Fig. 9 (c) to Fig. 8 (c) , the area with high-angle misorientation increases in Fig. 9 (c). As the reason, it is considered that the highly localized orientation gradient at around sides of triangular elements causes such high misorientation through Eq. 12. Finally, the subgrain size on all grid points are determined by Eq. 10 using smoothed stored energy and calculated misorientation. The subgrain diameters calculated at all grid points are the range 0.97 to 3.46 μm.

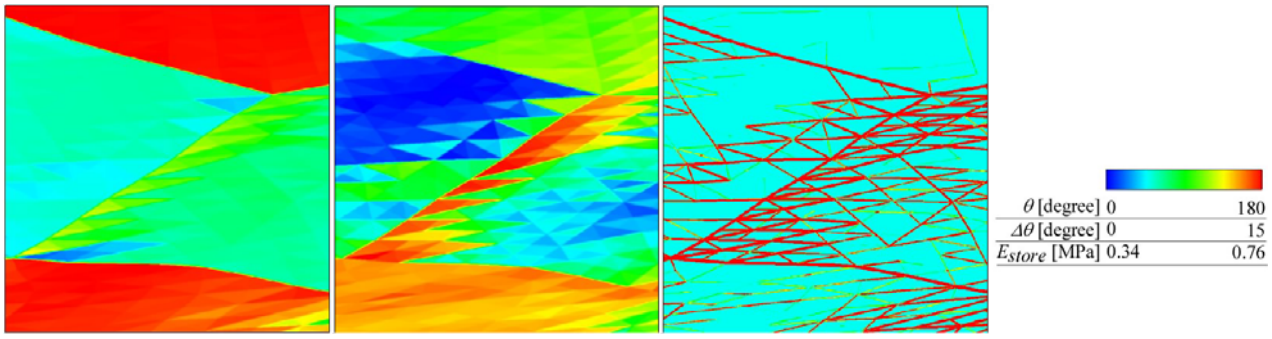

(a) *(b)* *(c)*

Fig. 9 Smoothed results of (a) crystal orientation θ and (b) stored energy E_{store} and (c) misorientation $\Delta\theta$ calculated by Eq. 12

The nuclei are sowed so as that the circular subgrains with diameter D_s of grid points selected randomly fill the computational domain. The distributes of created 2229 nuclei are shown in Fig. 10 (a). From these nuclei, the normal grain growth is simulated to obtain the subgrain structures. Figures 9 (a), (b) and (c) are the time slices during the simulation. Figures 9 (c) and (d) are the predicted subgrain structures, where (d) indicates grain boundaries and crystal orientations. From Fig. 9 (d), the crystal orientations are almost same with Fig. 9 (a). The small subgrains are observed at the area where the stored energy is high. Therefore, it is confirmed that the plausible subgrain structures can be predicted by the proposed model.

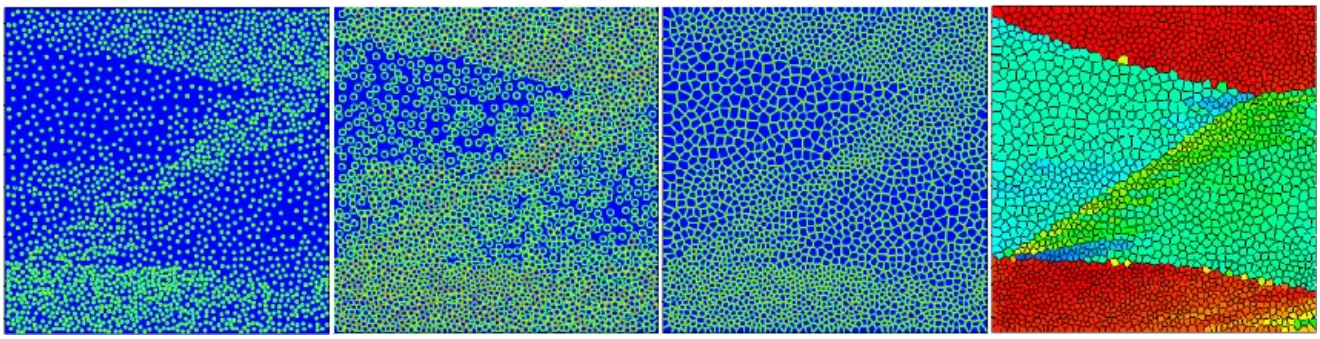

(a) (b) (c) (d)

Fig. 10 (a) Nuclei sowed randomly, (b) during grain growth simulation to prepare subgrain structure, (c) predicted subgrain structures and (d) its crystal orientations

The static recrystallization simulation is carried out from the predicted subgrain structures shown in Fig. 9 (d). The computational domain size is 80 μm x 80 μm (800 x 800 grids) with grid size $\Delta x = 0.1$ μm. Zero Neumann boundary conditions are applied for all sides of computational domain. The other conditions are as follows: the interface thickness $\delta = 7\Delta x$, interface energy $\gamma = 0.6$ J/m^2, time increment $\Delta t = 0.05$ s and grain boundary mobility $M = M_0 \exp(-Q/kT)$ where pre-exponential factor $M_0 = 6.2 \times 10^{-6}$ m^2/Ns, activation energy $Q = 2.08 \times 10^{-19}$ J, Boltzmann constant $k = 1.38 \times 10^{-23}$ J/K and temperature $T = 800$ K [13].

Figure 11 shows the time evolution of subgrain structures and the growth of recrystallized grains during annealing. At the beginning of simulation, the high-angle grain boundaries become smooth owing to their curvature, as can be seen in Fig. 11 (a) with comparing to Fig. 10 (d). After then, some grains with high-angle boundaries grow abnormally and become recrystallized grains. In particular, large recrystallized grains grow into upper and lower grains, because their two grains are deformed intensely and have small subgrain structures. The large deformation area on the diagonal line of computational domain is also preferred nucleation site. However, since the deformation is localized around the diagonal line, the growth rate of recrystallized grains is slower than those of upper and lower regions. In the large initial subgrain regions in Fig. 10 (d), no recrystallization occurs in this simulation period. As a result, the spontaneous nucleation by abnormal grain growth and the recrystallized grain growth depending on the deformation structures are observed in the present model developed here.

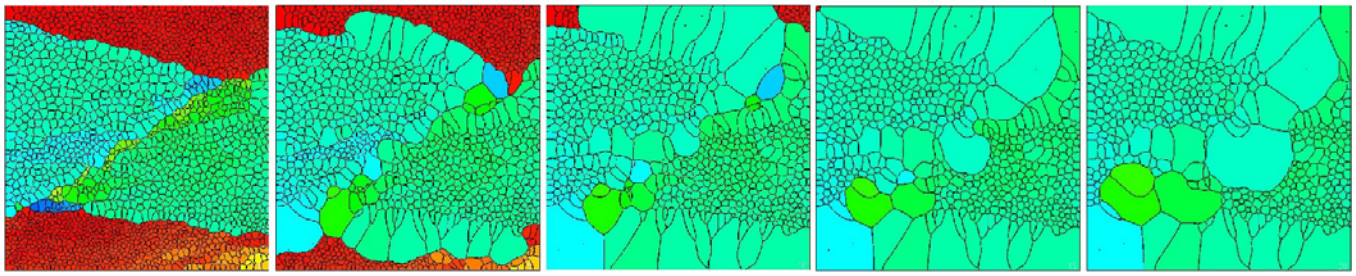

(a) (b) (c) (d) (e)

Fig. 11 Time evolution during static recrystallization simulation at (a) 300, (b) 1500, (c) 3000, (d) 4500 and (e) 6000 s

CONCLUSIONS

We developed a coupled model for static recrystallization of the phase-field method and crystal plasticity finite element method. In this model, the subgrain structures are predicted from crystal orientation and stored energy calculated by crystal plasticity finite element simulation. The multi-phase-field model proposed is employed as a grain growth model and the misorientation dependency of grain boundary energy and mobility are introduced into the phase-field model to reproduce abnormal grain growth which enable spontaneous nucleation. By performing a series of procedure, it is confirmed that the proposed model can predict the desired subgrain structures depending on the stored energy and crystal orientation distribution. Furthermore, during static recrystallization simulation, spontaneous nucleation by abnormal grain growth and the growth of recrystallized grain depending on the deformation microstructures are confirmed.

Acknowledgements Financial support from the Ministry of Education, Culture, Sports, Science and Technology of Japan through a Grant-in-Aid for Scientific Research is highly appreciated.

REFERENCES

[1] M. A. Miodownik, *A review of microstructural computer models used to simulate grain growth and recrystallisation in aluminium alloys*, J. Light Metals Vol. 2-3 (2002), 125-135.

[2] D. J. Srolovitz, G. S. Grest, M. P. Anderson, *Computer simulation of recrystallization—I. Homogeneous nucleation and growth,* Acta metal., 34, (1986), 1833-1845.

[3] H. W. Hesselbarth, I. R. Göbel, *Simulation of recrystallization by cellular automata*, Acta Metall. Mater., 39, (1991), 2135-2143.

[4] T. Takaki, Y. Yamanaka, Y. Higa, Y. Tomita, *Phase-Field Model during Static Recrystallization based on Crystal-Plasticity Theory*, Scientific Modeling and Simulation, (2008), accepted.

[5] Y. Suwa, Y. Saito, H. Onodera, *Phase field simulation of stored energy driven interface migration at a recrystallization front*, Mater. Sci. Eng. A, 457, (2007), 132-138.

[6] D. Raabe, L. Hantcherli, *2D cellular automaton simulation of the recrystallization texture of an IF sheet steel under consideration of Zener pinning*, Comp. Mater. Sci., 34, (2005), 299-313.

[7] D. Raabe, R. C. Becker, *Coupling of a Crystal Plasticity Finite Element Model with a Probabilistic Cellular Automaton for Simulating Primary Static Recrystallization in Aluminum*, Model. Simul. Mater. Sci. Eng., 8, (2000), 445-462.

[8] F. J. Humphreys, *A unified theory of recovery, recrystallization and grain growth, based on the stability and growth of cellular microstructures—I. The basic model*, Acta Mater., 45, (1997), 4231-4240.

[9] I. Steinbach, F. Pezzolla, *A generalized field method for multiphase transformations using interface fields*, Physica D, 134, (1999), 385-393.

[10] S. G. Kim, D. I. Kim, W. T. Kim, Y. B. Park, *Computer simulations of two-dimensional and three-dimensional ideal grain growth*, Phys. Rev. E, 74, (2006), 061605-1-061605-14.

[11] T. Takaki, A. Yamanaka, Y. Tomita, *Phase-Field Modeling for Dynamic Recrystallization*, Proceeding of International Conference on Advances and Trends in Engineering Materials and their Applications, (2007), in press.

[12] F. J. Humphreys, M. Hatherly, *Recrystallization and Related Annealing Phenomena*, Elsevier, (2004).

[13] D. Raabe, *Cellular automata in materials science with particular reference to recrystallization simulation*, Ann. Rev. Mater. Res., 32, (2002), 53-76.

[14] T. Takaki, A. Yamanaka, Y. Higa, Y. Tomita, *Development of Phase-Field Model and Computational Procedure During Static Primary Recrystallization*, Trans. J. Soc. Mech. Eng., 73, (2007), 482-489. (in Japanese)